EUROPEAN ORGANIZATION FOR NUCLEAR RESEARCH

CERN–PPE/95–60

3 May 1995

# A Measurement of $B^+$ and $B^0$ Lifetimes using $\overline{D}\ell^+$ events

DELPHI Collaboration

**Abstract**

A measurement of B meson lifetimes is presented using data collected from 1991 to 1993 by the DELPHI detector at the LEP collider. Samples of events with a D meson and a lepton in the same jet are selected where $\overline{D}^0\ell^+$ and $D^{*-}\ell^+$ events originate mainly from the semileptonic decays of $B^+$ and $B^0$ mesons, respectively. From the reconstructed B decay length and the estimated B momentum, taking into account the dilution due to B decays into $\overline{D}^{**}\ell^+\nu$, the following B meson lifetimes and lifetime ratio are measured:

$$\begin{aligned} \tau(B^+) &= 1.61^{+0.16}_{-0.16}\ (\text{stat.}) \pm 0.12\ (\text{syst.})\ \text{ps} \\ \tau(B^0) &= 1.61^{+0.14}_{-0.13}\ (\text{stat.}) \pm 0.08\ (\text{syst.})\ \text{ps} \\ \tau(B^+)/\tau(B^0) &= 1.00^{+0.17}_{-0.15}\ (\text{stat.}) \pm 0.10\ (\text{syst.}) \end{aligned}$$

and an average lifetime of $B^+$ and $B^0$ mesons is obtained:

$$\tau(B) = 1.61^{+0.08}_{-0.07}\ (\text{stat.}) \pm 0.05\ (\text{syst.})\ \text{ps}$$

(To be submitted to Zeit. Phys. C)

P.Abreu[21], W.Adam[50], T.Adye[37], E.Agasi[31], I.Ajinenko[42], R.Aleksan[39], G.D.Alekseev[16], P.P.Allport[22], S.Almehed[24], S.J.Alvsvaag[4], U.Amaldi[9], S.Amato[47], A.Andreazza[28], M.L.Andrieux[14], P.Antilogus[25], W-D.Apel[17], Y.Arnoud[39], B.Åsman[44], J-E.Augustin[19], A.Augustinus[31], P.Baillon[9], P.Bambade[19], F.Barao[21], R.Barate[14], G.Barbiellini[46], D.Y.Bardin[16], G.J.Barker[35], A.Baroncelli[40], O.Barring[24], J.A.Barrio[26], W.Bartl[50], M.J.Bates[37], M.Battaglia[15], M.Baubillier[23], J.Baudot[39], K-H.Becks[52], M.Begalli[6], P.Beilliere[8], Yu.Belokopytov[9], A.C.Benvenuti[5], M.Berggren[41], D.Bertrand[2], F.Bianchi[45], M.Bigi[45], M.S.Bilenky[16], P.Billoir[23], D.Bloch[10], M.Blume[52], S.Blyth[35], V.Bocci[38], T.Bolognese[39], M.Bonesini[28], W.Bonivento[28], P.S.L.Booth[22], G.Borisov[42], C.Bosio[40], S.Bosworth[35], O.Botner[48], B.Bouquet[19], C.Bourdarios[9], T.J.V.Bowcock[22], M.Bozzo[13], P.Branchini[40], K.D.Brand[36], R.A.Brenner[15], C.Bricman[2], L.Brillault[23], R.C.A.Brown[9], P.Bruckman[18], J-M.Brunet[8], L.Bugge[33], T.Buran[33], A.Buys[9], M.Caccia[28], M.Calvi[28], A.J.Camacho Rozas[41], T.Camporesi[9], V.Canale[38], M.Canepa[13], K.Cankocak[44], F.Cao[2], F.Carena[9], P.Carrilho[47], L.Carroll[22], C.Caso[13], M.V.Castillo Gimenez[49], A.Cattai[9], F.R.Cavallo[5], L.Cerrito[38], V.Chabaud[9], M.Chapkin[42], Ph.Charpentier[9], L.Chaussard[25], J.Chauveau[23], P.Checchia[36], G.A.Chelkov[16], R.Chierici[45], P.Chliapnikov[42], P.Chochula[7], V.Chorowicz[9], V.Cindro[43], P.Collins[9], J.L.Contreras[19], R.Contri[13], E.Cortina[49], G.Cosme[19], F.Cossutti[46], H.B.Crawley[1], D.Crennell[37], G.Crosetti[13], J.Cuevas Maestro[34], S.Czellar[15], E.Dahl-Jensen[29], J.Dahm[52], B.Dalmagne[19], M.Dam[33], G.Damgaard[29], A.Daum[17], P.D.Dauncey[37], M.Davenport[9], W.Da Silva[23], C.Defoix[8], G.Della Ricca[46], P.Delpierre[27], N.Demaria[35], A.De Angelis[9], H.De Boeck[2], W.De Boer[17], S.De Brabandere[2], C.De Clercq[2], C.De La Vaissiere[23], B.De Lotto[46], A.De Min[28], L.De Paula[47], C.De Saint-Jean[39], H.Dijkstra[9], L.Di Ciaccio[38], F.Djama[10], J.Dolbeau[8], M.Donszelmann[9], K.Doroba[51], M.Dracos[10], J.Drees[52], K.-A.Drees[52], M.Dris[32], Y.Dufour[8], F.Dupont[14], D.Edsall[1], R.Ehret[17], G.Eigen[4], T.Ekelof[48], G.Ekspong[44], M.Elsing[52], J-P.Engel[10], N.Ershaidat[23], B.Erzen[43], E.Falk[24], D.Fassouliotis[32], M.Feindt[9], A.Fenyuk[42], A.Ferrer[49], T.A.Filippas[32], A.Firestone[1], P.-A.Fischer[10], H.Foeth[9], E.Fokitis[32], F.Fontanelli[13], F.Formenti[9], B.Franek[37], P.Frenkiel[8], D.C.Fries[17], A.G.Frodesen[4], R.Fruhwirth[50], F.Fulda-Quenzer[19], H.Furstenau[9], J.Fuster[49], A.Galloni[22], D.Gamba[45], M.Gandelman[6], C.Garcia[49], J.Garcia[41], C.Gaspar[9], U.Gasparini[36], Ph.Gavillet[9], E.N.Gazis[32], D.Gele[10], J-P.Gerber[10], M.Gibbs[22], D.Gillespie[9], R.Gokieli[51], B.Golob[43], G.Gopal[37], L.Gorn[1], M.Gorski[51], Yu.Gouz[42], V.Gracco[13], E.Graziani[40], G.Grosdidier[19], P.Gunnarsson[44], M.Gunther[48], J.Guy[37], U.Haedinger[17], F.Hahn[52], M.Hahn[17], S.Hahn[52], Z.Hajduk[18], A.Hallgren[48], K.Hamacher[52], W.Hao[31], F.J.Harris[35], V.Hedberg[24], R.Henriques[21], J.J.Hernandez[49], P.Herquet[2], H.Herr[9], T.L.Hessing[9], E.Higon[49], H.J.Hilke[9], T.S.Hill[1], S-O.Holmgren[44], P.J.Holt[35], D.Holthuizen[31], M.Houlden[22], J.Hrubec[50], K.Huet[2], K.Hultqvist[44], P.Ioannou[3], J.N.Jackson[22], R.Jacobsson[44], P.Jalocha[18], R.Janik[7], G.Jarlskog[24], P.Jarry[39], B.Jean-Marie[19], E.K.Johansson[44], L.Jonsson[24], P.Jonsson[24], C.Joram[9], P.Juillot[10], M.Kaiser[17], G.Kalmus[37], F.Kapusta[23], M.Karlsson[44], E.Karvelas[11], S.Katsanevas[3], E.C.Katsoufis[32], R.Keranen[15], B.A.Khomenko[16], N.N.Khovanski[16], B.King[22], N.J.Kjaer[29], H.Klein[9], A.Klovning[4], P.Kluit[31], J.H.Koehne[17], B.Koene[31], P.Kokkinias[11], M.Koratzinos[9], V.Kostioukhine[42], C.Kourkoumelis[3], O.Kouznetsov[13], P.-H.Kramer[52], M.Krammer[50], C.Kreuter[17], J.Krolikowski[51], I.Kronkvist[24], Z.Krumstein[16], W.Krupinski[18], P.Kubinec[7], W.Kucewicz[18], K.Kurvinen[15], C.Lacasta[49], I.Laktineh[25], S.Lamblot[23], J.W.Lamsa[1], L.Lanceri[46], D.W.Lane[1], P.Langefeld[52], I.Last[22], J-P.Laugier[39], R.Lauhakangas[15], G.Leder[50], F.Ledroit[14], V.Lefebure[2], C.K.Legan[1], R.Leitner[30], Y.Lemoigne[39], J.Lemonne[2], G.Lenzen[52], V.Lepeltier[19], T.Lesiak[36], D.Liko[50], R.Lindner[52], A.Lipniacka[19], I.Lippi[36], B.Loerstad[24], M.Lokajicek[12], J.G.Loken[35], J.M.Lopez[41], A.Lopez-Fernandez[9], M.A.Lopez Aguera[41], D.Loukas[11], P.Lutz[39], L.Lyons[35], J.MacNaughton[50], G.Maehlum[17], A.Maio[21], V.Malychev[16], F.Mandl[50], J.Marco[41], B.Marechal[47], M.Margoni[36], J-C.Marin[9], C.Mariotti[40], A.Markou[11], T.Maron[52], C.Martinez-Rivero[41], F.Martinez-Vidal[49], S.Marti i Garcia[49], F.Matorras[41], C.Matteuzzi[28], G.Matthiae[38], M.Mazzucato[36], M.Mc Cubbin[9], R.Mc Kay[1], R.Mc Nulty[22], J.Medbo[48], C.Meroni[28], W.T.Meyer[1], M.Michelotto[36], E.Migliore[45], L.Mirabito[25], W.A.Mitaroff[50], U.Mjoernmark[24], T.Moa[44], R.Moeller[29], K.Moenig[9], M.R.Monge[13], P.Morettini[13], H.Mueller[17], L.M.Mundim[6], W.J.Murray[37], B.Muryn[18], G.Myatt[35], F.Naraghi[14], F.L.Navarria[5], S.Navas[49], P.Negri[28], S.Nemecek[12], W.Neumann[52], R.Nicolaidou[3], B.S.Nielsen[29], M.Nieuwenhuizen[31], V.Nikolaenko[10], P.Niss[44], A.Nomerotski[36], A.Normand[35], W.Oberschulte-Beckmann[17], V.Obraztsov[42], A.G.Olshevski[16], A.Onofre[21], R.Orava[15], K.Osterberg[15], A.Ouraou[39], P.Paganini[19], M.Paganoni[28], P.Pages[10], H.Palka[18], Th.D.Papadopoulou[32], L.Pape[9], C.Parkes[35], F.Parodi[13], A.Passeri[40], M.Pegoraro[36], L.Peralta[21], H.Pernegger[50], M.Pernicka[50], A.Perrotta[5], C.Petridou[46], A.Petrolini[13], H.T.Phillips[37], G.Piana[13], F.Pierre[39], M.Pimenta[21], S.Plaszczynski[19], O.Podobrin[17], M.E.Pol[6], G.Polok[18], P.Poropat[46], V.Pozdniakov[16], M.Prest[46], P.Privitera[38], N.Pukhaeva[16], A.Pullia[28], D.Radojicic[35], S.Ragazzi[28], H.Rahmani[32], J.Rames[12], P.N.Ratoff[20], A.L.Read[33], M.Reale[52], P.Rebecchi[19], N.G.Redaelli[28], M.Regler[50], D.Reid[9], P.B.Renton[35], L.K.Resvanis[3], F.Richard[19], J.Richardson[22], J.Ridky[12], G.Rinaudo[45], I.Ripp[39], A.Romero[45], I.Roncagliolo[13], P.Ronchese[36], V.Ronjin[42], L.Roos[14], E.I.Rosenberg[1], E.Rosso[9], P.Roudeau[19], T.Rovelli[5], W.Ruckstuhl[31], V.Ruhlmann-Kleider[39], A.Ruiz[41], H.Saarikko[15], Y.Sacquin[39], A.Sadovsky[16], G.Sajot[14], J.Salt[49], J.Sanchez[26], M.Sannino[13], H.Schneider[17], M.A.E.Schyns[52], G.Sciolla[45], F.Scuri[46], Y.Sedykh[16], A.M.Segar[35], A.Seitz[17], R.Sekulin[37], R.C.Shellard[6], I.Siccama[31], P.Siegrist[39], S.Simonetti[39], F.Simonetto[36], A.N.Sisakian[16], B.Sitar[7], T.B.Skaali[33], G.Smadja[25], N.Smirnov[42], O.Smirnova[16], G.R.Smith[37], O.Solovyanov[42], R.Sosnowski[51], D.Souza-Santos[6], T.Spassov[21], E.Spiriti[40], S.Squarcia[13], H.Staeck[52], C.Stanescu[40], S.Stapnes[33], I.Stavitski[36], K.Stepaniak[51], F.Stichelbaut[9], A.Stocchi[19], J.Strauss[50], R.Strub[10], B.Stugu[4], M.Szczekowski[51], M.Szeptycka[51], T.Tabarelli[28], J.P.Tavernet[23], O.Tchikilev[42], A.Tilquin[27], J.Timmermans[31], L.G.Tkatchev[16], T.Todorov[10], D.Z.Toet[31],

A.Tomaradze[2], B.Tome[21], L.Tortora[40], G.Transtromer[24], D.Treille[9], W.Trischuk[9], G.Tristram[8], A.Trombini[19], C.Troncon[28], A.Tsirou[9], M-L.Turluer[39], I.A.Tyapkin[16], M.Tyndel[37], S.Tzamarias[22], B.Ueberschaer[52], S.Ueberschaer[52], O.Ullaland[9], V.Uvarov[42], G.Valenti[5], E.Vallazza[9], C.Vander Velde[2], G.W.Van Apeldoorn[31], P.Van Dam[31], W.K.Van Doninck[2], J.Van Eldik[31], N.Vassilopoulos[35], G.Vegni[28], L.Ventura[36], W.Venus[37], F.Verbeure[2], M.Verlato[36], L.S.Vertogradov[16], D.Vilanova[39], P.Vincent[25], L.Vitale[46], E.Vlasov[42], A.S.Vodopyanov[16], V.Vrba[12], H.Wahlen[52], C.Walck[44], F.Waldner[46], A.Wehr[52], M.Weierstall[52], P.Weilhammer[9], A.M.Wetherell[9], D.Wicke[52], J.H.Wickens[2], M.Wielers[17], G.R.Wilkinson[35], W.S.C.Williams[35], M.Winter[10], M.Witek[9], K.Woschnagg[48], K.Yip[35], O.Yushchenko[42], F.Zach[25], C.Zacharatou[24], A.Zalewska[18], P.Zalewski[51], D.Zavrtanik[43], E.Zevgolatakos[11], N.I.Zimin[16], M.Zito[39], D.Zontar[43], R.Zuberi[35], G.C.Zucchelli[44], G.Zumerle[36]

[1] Ames Laboratory and Department of Physics, Iowa State University, Ames IA 50011, USA
[2] Physics Department, Univ. Instelling Antwerpen, Universiteitsplein 1, B-2610 Wilrijk, Belgium
and IIHE, ULB-VUB, Pleinlaan 2, B-1050 Brussels, Belgium
and Faculté des Sciences, Univ. de l'Etat Mons, Av. Maistriau 19, B-7000 Mons, Belgium
[3] Physics Laboratory, University of Athens, Solonos Str. 104, GR-10680 Athens, Greece
[4] Department of Physics, University of Bergen, Allégaten 55, N-5007 Bergen, Norway
[5] Dipartimento di Fisica, Università di Bologna and INFN, Via Irnerio 46, I-40126 Bologna, Italy
[6] Centro Brasileiro de Pesquisas Físicas, rua Xavier Sigaud 150, RJ-22290 Rio de Janeiro, Brazil
and Depto. de Física, Pont. Univ. Católica, C.P. 38071 RJ-22453 Rio de Janeiro, Brazil
and Inst. de Física, Univ. Estadual do Rio de Janeiro, rua São Francisco Xavier 524, Rio de Janeiro, Brazil
[7] Comenius University, Faculty of Mathematics and Physics, Mlynska Dolina, SK-84215 Bratislava, Slovakia
[8] Collège de France, Lab. de Physique Corpusculaire, IN2P3-CNRS, F-75231 Paris Cedex 05, France
[9] CERN, CH-1211 Geneva 23, Switzerland
[10] Centre de Recherche Nucléaire, IN2P3 - CNRS/ULP - BP20, F-67037 Strasbourg Cedex, France
[11] Institute of Nuclear Physics, N.C.S.R. Demokritos, P.O. Box 60228, GR-15310 Athens, Greece
[12] FZU, Inst. of Physics of the C.A.S. High Energy Physics Division, Na Slovance 2, 180 40, Praha 8, Czech Republic
[13] Dipartimento di Fisica, Università di Genova and INFN, Via Dodecaneso 33, I-16146 Genova, Italy
[14] Institut des Sciences Nucléaires, IN2P3-CNRS, Université de Grenoble 1, F-38026 Grenoble Cedex, France
[15] Research Institute for High Energy Physics, SEFT, P.O. Box 9, FIN-00014 Helsinki, Finland
[16] Joint Institute for Nuclear Research, Dubna, Head Post Office, P.O. Box 79, 101 000 Moscow, Russian Federation
[17] Institut für Experimentelle Kernphysik, Universität Karlsruhe, Postfach 6980, D-76128 Karlsruhe, Germany
[18] High Energy Physics Laboratory, Institute of Nuclear Physics, Ul. Kawiory 26a, PL-30055 Krakow 30, Poland
[19] Université de Paris-Sud, Lab. de l'Accélérateur Linéaire, IN2P3-CNRS, Bat 200, F-91405 Orsay Cedex, France
[20] School of Physics and Materials, University of Lancaster, Lancaster LA1 4YB, UK
[21] LIP, IST, FCUL - Av. Elias Garcia, 14-1°, P-1000 Lisboa Codex, Portugal
[22] Department of Physics, University of Liverpool, P.O. Box 147, Liverpool L69 3BX, UK
[23] LPNHE, IN2P3-CNRS, Universités Paris VI et VII, Tour 33 (RdC), 4 place Jussieu, F-75252 Paris Cedex 05, France
[24] Department of Physics, University of Lund, Sölvegatan 14, S-22363 Lund, Sweden
[25] Université Claude Bernard de Lyon, IPNL, IN2P3-CNRS, F-69622 Villeurbanne Cedex, France
[26] Universidad Complutense, Avda. Complutense s/n, E-28040 Madrid, Spain
[27] Univ. d'Aix - Marseille II - CPP, IN2P3-CNRS, F-13288 Marseille Cedex 09, France
[28] Dipartimento di Fisica, Università di Milano and INFN, Via Celoria 16, I-20133 Milan, Italy
[29] Niels Bohr Institute, Blegdamsvej 17, DK-2100 Copenhagen 0, Denmark
[30] NC, Nuclear Centre of MFF, Charles University, Areal MFF, V Holesovickach 2, 180 00, Praha 8, Czech Republic
[31] NIKHEF-H, Postbus 41882, NL-1009 DB Amsterdam, The Netherlands
[32] National Technical University, Physics Department, Zografou Campus, GR-15773 Athens, Greece
[33] Physics Department, University of Oslo, Blindern, N-1000 Oslo 3, Norway
[34] Dpto. Fisica, Univ. Oviedo, C/P. Pérez Casas, S/N-33006 Oviedo, Spain
[35] Department of Physics, University of Oxford, Keble Road, Oxford OX1 3RH, UK
[36] Dipartimento di Fisica, Università di Padova and INFN, Via Marzolo 8, I-35131 Padua, Italy
[37] Rutherford Appleton Laboratory, Chilton, Didcot OX11 OQX, UK
[38] Dipartimento di Fisica, Università di Roma II and INFN, Tor Vergata, I-00173 Rome, Italy
[39] Centre d'Etude de Saclay, DSM/DAPNIA, F-91191 Gif-sur-Yvette Cedex, France
[40] Istituto Superiore di Sanità, Ist. Naz. di Fisica Nucl. (INFN), Viale Regina Elena 299, I-00161 Rome, Italy
[41] C.E.A.F.M., C.S.I.C. - Univ. Cantabria, Avda. los Castros, S/N-39006 Santander, Spain, (CICYT-AEN93-0832)
[42] Inst. for High Energy Physics, Serpukov P.O. Box 35, Protvino, (Moscow Region), Russian Federation
[43] J. Stefan Institute and Department of Physics, University of Ljubljana, Jamova 39, SI-61000 Ljubljana, Slovenia
[44] Fysikum, Stockholm University, Box 6730, S-113 85 Stockholm, Sweden
[45] Dipartimento di Fisica Sperimentale, Università di Torino and INFN, Via P. Giuria 1, I-10125 Turin, Italy
[46] Dipartimento di Fisica, Università di Trieste and INFN, Via A. Valerio 2, I-34127 Trieste, Italy
and Istituto di Fisica, Università di Udine, I-33100 Udine, Italy
[47] Univ. Federal do Rio de Janeiro, C.P. 68528 Cidade Univ., Ilha do Fundão BR-21945-970 Rio de Janeiro, Brazil
[48] Department of Radiation Sciences, University of Uppsala, P.O. Box 535, S-751 21 Uppsala, Sweden
[49] IFIC, Valencia-CSIC, and D.F.A.M.N., U. de Valencia, Avda. Dr. Moliner 50, E-46100 Burjassot (Valencia), Spain
[50] Institut für Hochenergiephysik, Österr. Akad. d. Wissensch., Nikolsdorfergasse 18, A-1050 Vienna, Austria
[51] Inst. Nuclear Studies and University of Warsaw, Ul. Hoza 69, PL-00681 Warsaw, Poland
[52] Fachbereich Physik, University of Wuppertal, Postfach 100 127, D-42097 Wuppertal 1, Germany

# 1 Introduction

According to the spectator model of b-hadron weak decays, all b-hadrons should have the same lifetime [1]. QCD corrections based on an expansion in inverse powers of the b quark mass predict non-spectator contributions to the inclusive B partial width to be proportional to $(f_B/m_B)^2$ where $f_B$ is the B decay constant [2]. Due to mass effects, the predicted lifetime ratios are thus close to unity [†] :

$$\tau(B^+)/\tau(B^0) = 1 + 0.05 \cdot (f_B/200\ \mathrm{MeV})^2,\ \tau(B_s^0)/\tau(B^0) \simeq 1,\ \tau(\Lambda_b^0)/\tau(B^0) \sim 0.9\ , \quad (1)$$

and it is very unlikely that the lifetime of the charged B meson exceeds the lifetime of the neutral B meson by more than 10%.

Despite the fact that the average b-hadron lifetime is now precisely measured ($\tau(B) = 1.537 \pm 0.021$ ps [3]), the published measurements of individual B lifetimes do not allow the relations in equation (1) to be tested to better than 7% accuracy [4].

In the charm quark sector, the observed lifetime ratios [3] differ significantly from the naive spectator model prediction :

$$\tau(D^+)/\tau(D^0) = 2.55 \pm 0.04,\ \tau(D_s^+)/\tau(D^0) = 1.13 \pm 0.04,\ \tau(\Lambda_c^+)/\tau(D^0) = 0.48 \pm 0.03.$$

Weak annihilation and Pauli interference processes have to be introduced to explain these different lifetimes.

This paper presents an updated measurement of the $B^+$ and $B^0$ lifetimes using events with a charmed meson and a lepton produced in B meson semileptonic decays. In these events, the $B^+$ meson decays semileptonically into $\overline{D}^0\ell^+\nu$, $\overline{D}^{*0}\ell^+\nu$ or $\overline{D}^{**0}\ell^+\nu$ and the $B^0$ into $D^-\ell^+\nu$, $D^{*-}\ell^+\nu$ or $D^{**-}\ell^+\nu$ [‡]. For the lifetime measurements in this paper, the decay modes $B^+ \to \overline{D}^0\ell^+X$ and $B^0 \to D^{*-}\ell^+X$ are used. Because of $\overline{D}^{**}$ decays into a $\overline{D}^{(*)0}$ or into a $D^{(*)-}$ in the final state, the $B^+$ and $B^0$ purities in the $\overline{D}^0\ell^+X$ and $D^{*-}\ell^+X$ samples are diluted. This effect has to be taken into account in the extraction of the lifetimes.

Data were selected from $Z^0$ hadronic decays collected at LEP by the DELPHI experiment in 1991-1993. Compared to a previous publication [5], the present paper benefits from a larger statistics and reduced systematic uncertainties. Charmed mesons were reconstructed if an identified lepton was produced in the same jet by any of the following decays :

- $\overline{D}^0 \to K^+\pi^-$ or $K^+\pi^-\pi^-\pi^+$;
- $D^{*-} \to \overline{D}^0\pi^-$ followed by $\overline{D}^0 \to K^+\pi^-$ , or $K^+\pi^-\pi^-\pi^+$ or $K^+\pi^-\pi^0$ where the $\pi^0$ was not reconstructed.

After a brief description of the DELPHI detector, the criteria for selecting hadronic $Z^0$ events and for identifying leptons and kaons are explained in section 2. The vertex reconstructions and selections made for the different D decay modes are detailed in section 3. The B meson lifetime measurement is described in section 4 for each individual $\overline{D}\ell^+$ channel and an average lifetime of $B^+$ and $B^0$ mesons is presented. Finally, taking into account the dilution due to B decays into $\overline{D}^{**}\ell^+\nu$ , the charged and neutral B lifetimes are given in section 5 from the measured $\overline{D}^0\ell^+$ and $D^{*-}\ell^+$ events, respectively, and the lifetime ratio is obtained.

[†] Throughout the paper the notation $B^0$ refers uniquely to the $B_d^0$ meson, and charge-conjugate states are implicitly included.

[‡] In the following $D^{(*)}$ will mean D or D* and $D^{(*)(*)}$ will mean D, D* or D**, where D** denotes any charm meson orbitally excited state or nonresonant $D^{(*)}n\pi$ state.

# 2 Experimental procedure and event selection

A description of the DELPHI apparatus can be found in reference [6]. Only the components most relevant for this analysis are described here.

## 2.1 Tracking detectors and kaon identification

The tracking of charged particles is accomplished in the barrel region with a set of cylindrical tracking detectors whose axes are oriented along the 1.23 T magnetic field and the direction of the beam. The microvertex detector (VD), the inner detector (ID), the time projection chamber (TPC) and the outer detector (OD), measure the charged particle tracks at polar angles $\theta$ between 30° and 150°. Combining the information from these detectors, a resolution $\sigma(p)/p$ of $\pm 5.0$ % has been obtained for muons of 45 GeV/$c$ momentum. Hadrons are identified using the specific ionization in the TPC and the Cherenkov radiation in the barrel Ring Imaging CHerenkov detector (RICH) placed between the TPC and the OD detectors. The tracking in the forward ($11° < \theta < 33°$) and backward ($147° < \theta < 169°$) regions is assisted by two pairs of Forward drift Chambers (FCA and FCB) in the end-caps.

The microvertex detector [7] is made of three concentric cylindrical shells of silicon-strip detectors at radii of 6.3 cm, 9 cm and 11 cm covering the central region of the DELPHI apparatus at polar angles between 27° and 153°. The shells surround the beam pipe, a beryllium cylinder of inner radius 5.3 cm and wall thickness 1.45 mm. Each shell consists of 24 modules with about 10% overlap in azimuth between the modules. Each module holds 4 detectors with strips parallel to the beam direction. The silicon detectors are 300 $\mu$m thick and have a strip pitch of 25 $\mu$m. The read-out strips (50 $\mu$m pitch) are AC-coupled and give a 5 $\mu$m intrinsic precision on the coordinates of the charged particle tracks transverse to the beam direction. After a careful procedure of relative alignment of each single detector, an overall precision of 8 $\mu$m per point, in the plane perpendicular to the beam, has been achieved.

The TPC, the main tracking device, is a cylinder of 30 cm inner radius, 122 cm outer radius and length 2.7 m. For polar angles between 39° and 141° it provides up to 16 space points along the charged particle trajectory. The energy loss ($dE/dx$) for each charged particle is measured by the 192 TPC sense wires as the mean of the smallest 80% of the wire signals. Using $Z^0 \to \mu^+\mu^-$ events, the $dE/dx$ precision has been measured to be $\pm 5.5\%$. For particles in hadronic jets the precision is $\pm 7.5\%$, but for 25% of the particles the $dE/dx$ is not measured due to the presence of another charged particle within the two-track resolution distance of the TPC in the direction parallel to the beam. The mean $dE/dx$ for a kaon with momentum above 3 GeV/$c$ is about 1.6 standard deviations below the mean $dE/dx$ for a pion. In the following, a charged particle will be considered identified as a kaon if at least 30 TPC wires are used and if the measured $dE/dx$ is more than one standard deviation below the expected $dE/dx$ for a pion.

The fiducial volume of the barrel RICH detector [8] covers the polar angular acceptance of 47° to 133°. This ring imaging Cherenkov detector consists of two volumes in which the Cherenkov photons are produced, one filled with liquid $C_6F_{14}$ freon and the other with gaseous $C_5F_{12}$ freon. The 48 drift tubes containing a photo-sensitive agent (TMAE) are used for the photon detection. The RICH counter separates kaons from pions from 2.5 GeV/$c$ up to about 20 GeV/$c$ using the gas radiator. By adding the information from the liquid radiator, kaon identification is extended down to 1 GeV/$c$. The probabilities for the mass assignments were computed using the measured Cherenkov an-

gle and the number of detected photons. Kaon candidates were then selected on the basis of the pion and kaon probabilities. The kaon selection was defined in order to achieve a pion rejection factor [§] larger than 4. Identification with the liquid and gas radiators was possible for 20% and 60%, respectively, of the 1991-1993 data.

## 2.2 Calorimetry and lepton identification

Electron identification relies on the electromagnetic calorimeter in the barrel region (High density Projection Chamber HPC), situated inside the superconducting solenoid and covering polar angles between 43° and 137°. The detector has a thickness of 17.5 radiation lengths and consists of 144 modules arranged in 6 rings along the beam axis. Each module is divided into 9 drift layers separated by lead and provides three-dimensional shower reconstruction. For electrons with 45.6 GeV/$c$ momentum, the relative energy resolution was found to be $\pm 5.5\%$ with a spatial resolution along the beam axis of $\pm 2$ mm

For electron identification a fit was made to the longitudinal shower profile measured in the 9 HPC layers. In addition the energy, position and direction measurements of the shower in the HPC, together with the independent parameters from the track fit, were used to determine an overall probability for a shower to originate from an electron. The $dE/dx$ measurement in the TPC was used in addition to distinguish between electrons and hadrons. Photon conversions were discarded by rejecting all track pairs which formed a secondary vertex and whose invariant mass was compatible with zero. Finally, electrons were selected with momentum above 3 GeV/$c$ with an identification efficiency of $(77 \pm 5)\%$ for electrons within jets. The misidentification probability was less than 1.6%.

The muon identification relies mainly on the muon chambers, a set of drift chambers with three-dimensional information situated at the periphery of DELPHI after approximately 1 m of iron. In the Barrel part of the detector ($51° < \theta < 129°$) there are three layers each including two active planes of chambers. One set of chambers is located 20 cm before the end of the hadronic calorimeter [6], two further sets of chambers being outside. The two external layers overlap in azimuth to avoid dead spaces. Near 90° to the beam, there are 7.5 absorption lengths between the interaction point and the last muon detector. In the Forward part, two layers consist each of two planes of drift chambers with anode wires crossed at right angles.

Muon candidates with momentum above 3 GeV/$c$ were selected by extrapolating charged particle tracks through the calorimeters and performing a $\chi^2$ fit to the positions of hits in the muon chambers. Track measurement errors, multiple scattering errors and chamber resolutions were included. Within the geometrical and kinematical acceptance, an identification efficiency of $(91 \pm 4)\%$ was estimated using $Z^0 \to \mu^+\mu^-$, $\tau^- \to \mu^- X$ and $\gamma\gamma \to \mu^+\mu^-$ events. The misidentification probability was estimated to be $(1.1 \pm 0.1)\%$.

## 2.3 Event selection and simulation

Only charged particles were used in this analysis, with the following selection criteria: the momentum had to be between 0.4 GeV/$c$ and 50 GeV/$c$, the relative error on momentum measurement less than 100%, the track length in the TPC had to be larger than 30 cm, the projection of their impact parameter relative to the interaction point had to be below 4 cm in the plane transverse to the beam direction and the distance to the interaction point along the beam direction below 10 cm.

[§] The rejection factor is defined as the ratio of the probability for a real kaon to be correctly identified as a kaon to the probability for a real pion to be wrongly identified as a kaon.

Hadronic events were selected by requiring five or more charged particles and a total energy in charged particles larger than 12% of the collision energy, assuming all charged particles to be pions. A total of 1.7 million hadronic events was obtained from the 1991-1993 data.

Simulated hadronic events have been generated using the JETSET 7.3 Parton Shower program [9]. The B meson mean lifetime used was set to 1.6 ps. The generated events were followed through the detailed detector simulation DELSIM [10] which included simulation of secondary interactions and digitization of all electronic signals. The simulated data were then processed through the same analysis chain as the real data. The hadronic event selection efficiency was thus estimated to be (95.0±0.5)%. A total of 5.2 million simulated $Z^0$ hadronic decays was used.

Charged particles were clustered into jets using LUCLUS algorithm with default parameters [9]. For the jet containing the lepton candidate, the jet axis was defined as the sum of the momenta of all charged particles belonging to this jet not including the lepton. Then the transverse momentum, $p_T$, of the lepton with respect to this jet axis was required to be larger than 1 GeV/$c$.

# 3 Charmed meson reconstruction

The analysis of charmed mesons was based on the separation between primary and secondary vertices and on kaon identification.

## 3.1 Vertex selections

The primary interaction vertex was computed in space for each event using an iterative procedure based on the $\chi^2$ of the fit. The average transverse position of the interaction point, known for each fill, was included as a constraint during the primary vertex fit. The average widths of the beam overlap region, transverse to the beam axis, were taken to be 140 $\mu$m in the horizontal and 60 $\mu$m in the vertical directions (the latter is larger than the real beam dispersion in order to apply a looser constraint on the primary vertex fit). The overall $\chi^2$ divided by the number of charged particles used in the fit had to be less than 5. To achieve this, the charged particle with the largest $\chi^2$ contribution was discarded and a new primary vertex was computed. This procedure removed 30% of charged particles on average and provided primary vertex information for about 99% of events. For the remaining events, the primary vertex was computed using a selection of charged particles based on their impact parameters (defined in the plane transverse to the beam axis). The interaction vertex of $Z^0 \to b\overline{b}$ events was thus evaluated with a transverse resolution of about 70 $\mu$m in the horizontal and 30 $\mu$m in the vertical directions. Along the beam axis the resolution was about 500 $\mu$m.

Only charged particles produced in the same jet as the lepton were considered for the reconstruction of charmed mesons. The kaon candidate in D decay was required to have the same charge as the identified lepton.

Only particle tracks with at least one hit in the microvertex detector were used for the $\overline{D}^0$ reconstruction. A $K^+\pi^-$ or $K^+\pi^-\pi^-\pi^+$ combination was selected to compute a secondary vertex in space and the momentum vector of each particle was taken from this geometrical secondary vertex fit. The momentum of each particle had to be larger than 1 GeV/$c$. In the particular case of $\overline{D}^0 \to K3\pi$ decays, the minimum momentum required for pions was lowered to 0.2 GeV/$c$. In order to define more precisely the secondary

vertex for K3$\pi$ candidates, the impact parameter of each of these particles relative to the secondary vertex was required to be smaller than 100 $\mu$m for $\overline{\mathrm{D}}^0\ell^+$ events and 300 $\mu$m for $\mathrm{D}^{*-}\ell^+$ events.

Using a lepton candidate with at least one hit in the microvertex detector, a $\overline{\mathrm{D}}^0$-lepton vertex was then fitted in space, and the lepton momentum vector taken at this new vertex. The precision of this secondary vertex was found to be about $\pm$300 $\mu$m transverse to the beam direction.

All other charged particles with momentum between 0.4 GeV/$c$ and 4.5 GeV/$c$ and charge opposite to that of the lepton were used as pion candidates for $\mathrm{D}^{*-} \to \overline{\mathrm{D}}^0\pi^-$ decay. This momentum range allowed the selection of $\mathrm{D}^{*-}$ in the energy range defined in section 3.2. In order to reduce some backgrounds, without affecting the B lifetime measurement, the impact parameter of this pion relative to the primary interaction vertex was required to be less than 3.0 mm. The momentum vector of the pion candidate was taken at the previously defined $\overline{\mathrm{D}}^0$-lepton vertex. Then the selection of $\mathrm{D}^{*-}\ell^+X$ events relied on the small mass difference between the $\mathrm{D}^{*-}$ and the decaying $\overline{\mathrm{D}}^0$. The mass difference $\Delta M = M(\mathrm{K}\pi\pi) - M(\mathrm{K}\pi)$ was computed in case of a $\overline{\mathrm{D}}^0 \to \mathrm{K}^+\pi^-$ or $\mathrm{K}^+\pi^-(\pi^0)$ decay, and $\Delta M = M(\mathrm{K}3\pi\pi) - M(\mathrm{K}3\pi)$ in case of a $\overline{\mathrm{D}}^0 \to \mathrm{K}^+\pi^-\pi^-\pi^+$ decay.

## 3.2 $\overline{\mathrm{D}}\ell^+$ selections

The $\overline{\mathrm{D}}^0$ or $\mathrm{D}^{*-}$ meson was selected if its energy fraction $X_E(\mathrm{D}) = E(\mathrm{D})/E_{\mathrm{beam}}$ was larger than 0.15. In order to allow a reliable B momentum estimate, the $\overline{\mathrm{D}}\ell^+$ invariant mass was required to be between 2.80 GeV/$c^2$ and 5.28 GeV/$c^2$ in the K$\pi$ or K3$\pi$ modes, and between 2.80 GeV/$c^2$ and 5.14 GeV/$c^2$ for the $\mathrm{D}^{*-} \to \overline{\mathrm{D}}^0\pi^-$ with $\overline{\mathrm{D}}^0 \to \mathrm{K}^+\pi^-(\pi^0)$ decay channel. In case of $\mathrm{D}^{**}$ production where only the final state $\mathrm{D}^{(*)}$ was reconstructed, the $\overline{\mathrm{D}}^*\ell^+$ mass was lower than for a direct $\mathrm{D}^{(*)}$ production. The mass selection thus contributes to a reduction in the dilution due to $\mathrm{D}^{**}$ production (see section 5).

For the $\overline{\mathrm{D}}^0\ell^+X$ samples using $\overline{\mathrm{D}}^0 \to \mathrm{K}^+\pi^-$ and $\overline{\mathrm{D}}^0 \to \mathrm{K}^+\pi^-\pi^-\pi^+$ channels, the background was decreased by requiring the relative decay length $\Delta L/\sigma$ to be above 1 or 3, respectively. Here $\Delta L$ is defined as the signed distance between the primary and secondary $\overline{\mathrm{D}}^0$ vertices in the plane transverse to the beam axis. This distance is given the same sign as the scalar product of the $\overline{\mathrm{D}}^0$ momentum with the vector joining the primary to the secondary vertices. Using the microvertex detector, the resolution $\sigma$ on this transverse decay length is 250 $\mu$m on average.

To reduce the combinatorial background in the $\mathrm{D}^{*-}\ell^+$ and $\overline{\mathrm{D}}^0\ell^+$ samples further using the $\overline{\mathrm{D}}^0 \to \mathrm{K}^+\pi^-$ or $\mathrm{K}^+\pi^-(\pi^0)$ decay channels, the angle $\theta^*$ between the $\overline{\mathrm{D}}^0$ flight direction and the kaon direction in the $\overline{\mathrm{D}}^0$ rest frame was required to satisfy the condition $\cos\theta^* > -0.9$. For genuine $\overline{\mathrm{D}}^0 \to \mathrm{K}^+\pi^-$ candidates an isotropic distribution in $\cos\theta^*$ is expected whereas the background is strongly peaked in the backward direction.

Finally, kaon identification was required by using the $dE/dx$ or the RICH (see section 2.1). This criterion depended on the measured $X_E(\mathrm{D})$ and lepton $p_T$ and on the D decay channel considered in order to reduce the background while preserving a reasonable number of $\overline{\mathrm{D}}\ell^+$ candidates : it is summarized in tables 1 and 2 together with the other selections used.

The $\mathrm{D}^0$ and B proper times were measured as explained in section 4. The $\mathrm{D}^0$ proper time was required to be larger than -2 ps and the B proper time to lie between -2 and +10 ps.

| | $\overline{\mathrm{D}}^0 \to \mathrm{K}^+\pi^-$ | $\overline{\mathrm{D}}^0 \to \mathrm{K}^+\pi^-\pi^-\pi^+$ |
|---|---|---|
| $\cos\theta^*$ | $> -0.9$ | — |
| impact parameter | — | $< 100\ \mu$m |
| $\Delta L/\sigma$ of $\mathrm{D}^0$ | $> 1$ | $> 3$ |
| $0.15 < X_E < 0.35$ | K identification and $p_T > 1.5$ GeV/$c$ | |
| $0.35 < X_E < 1$ | K ident. or $p_T > 1.5$ GeV/$c$ | K identification |
| K$\pi$ or K3$\pi$ mass range | $m_{\mathrm{D}^0} \pm 50$ MeV/$c^2$ | $m_{\mathrm{D}^0} \pm 30$ MeV/$c^2$ |
| mass difference range | $\lvert\Delta m\rvert > 2$ MeV/$c^2$ | $\lvert\Delta m\rvert > 2$ MeV/$c^2$ |
| signal $\overline{\mathrm{D}}^0\ell^+$ events | $215 \pm 20$ | $162 \pm 19$ |
| fraction signal/total | $0.65 \pm 0.03$ | $0.57 \pm 0.04$ |

Table 1: Selection criteria and number of events for the $\overline{\mathrm{D}}^0\ell^+$ samples ($\Delta m$ stands for the $(M(\mathrm{K}n\pi\pi) - M(\mathrm{K}n\pi) - m_{\mathrm{D}^{*+}} + m_{\mathrm{D}^0})$ mass difference, where $n = 1$ or 3 according to the $\overline{\mathrm{D}}^0$ decay channel; $p_T$ is the transverse momentum of the lepton with respect to the jet axis).

| | $\overline{\mathrm{D}}^0 \to \mathrm{K}^+\pi^-$ | $\overline{\mathrm{D}}^0 \to \mathrm{K}^+\pi^-(\pi^0)$ | $\overline{\mathrm{D}}^0 \to \mathrm{K}^+\pi^-\pi^-\pi^+$ |
|---|---|---|---|
| $\cos\theta^*$ | $> -0.9$ | $> -0.9$ | — |
| impact parameter | — | — | $< 300\ \mu$m |
| $0.15 < X_E < 1$ | K identification or $p_T > 1.5$ GeV/$c$ | | |
| K$\pi$ or K3$\pi$ mass range | $m_{\mathrm{D}^0} \pm 50$ MeV/$c^2$ | 1550–1700 MeV/$c^2$ | $m_{\mathrm{D}^0} \pm 30$ MeV/$c^2$ |
| mass difference range | $\lvert\Delta m\rvert < 2$ MeV/$c^2$ | $\Delta M < 152$ MeV/$c^2$ | $\lvert\Delta m\rvert < 1.5$ MeV/$c^2$ |
| signal $\mathrm{D}^{*-}\ell^+$ events | $96 \pm 11$ | $92 \pm 13$ | $121 \pm 14$ |
| fraction signal/total | $0.92 \pm 0.03$ | $0.78 \pm 0.04$ | $0.69 \pm 0.04$ |

Table 2: Selection criteria and number of events for the $\mathrm{D}^{*-}\ell^+$ samples with $\mathrm{D}^{*-} \to \overline{\mathrm{D}}^0\pi^-$ decay ($\Delta m$ and $p_T$ are defined in table 1 caption).

### 3.3 Observed charm signal

The invariant K$\pi$ and K3$\pi$ mass distributions are presented in figures 1a) and b). Combinations with a mass difference value $\Delta M$ within 2 MeV/$c^2$ of the nominal $(\mathrm{D}^{*+} - \mathrm{D}^0)$ mass difference are removed. Similar distributions are shown in figure 1c) where the $\Delta M$ value is less than 152 MeV/$c^2$ and in figure 1d) where $\Delta M$ is within 1.5 MeV/$c^2$ of the nominal $(\mathrm{D}^{*+} - \mathrm{D}^0)$ mass difference. A clear signal corresponding to the $\mathrm{D}^0$ mass is observed in each distribution when the kaon candidate and the lepton have the same charge (data points). In figures 1a) and c) the contribution of the $\overline{\mathrm{D}}^0 \to \mathrm{K}^+\pi^-(\pi^0)$ decay (where the $\pi^0$ is not reconstructed) appears as a shoulder below 1.7 GeV/$c^2$.

No significant enhancement is observed for the corresponding wrong sign $\mathrm{K}^+\ell^-X$ events (hatched histograms), indicating a negligible contribution of $\mathrm{c\overline{c}}$ events. These signals in figures 1a) and b) are interpreted as $\mathrm{B} \to \overline{\mathrm{D}}^0\ell^+X$ events and those of figures 1c) and d) as $\mathrm{B} \to \mathrm{D}^{*-}\ell^+X$ events.

The K$\pi$ mass distributions of figures 1a) and c) were fitted by using the following contributions : an exponential function for the combinatorial background, a Gaussian

function for the $\overline{\mathrm{D}}^0 \to \mathrm{K}^+\pi^-$ events and a parameterization from the simulation of the $\overline{\mathrm{D}}^0 \to \mathrm{K}^+\pi^-(\pi^0)$ contribution below the $\mathrm{D}^0$ mass value. The K3$\pi$ mass distributions of figures 1b) and d) were fitted by using a second order polynomial for the combinatorial background and a Gaussian function for the $\overline{\mathrm{D}}^0 \to \mathrm{K}^+\pi^-\pi^-\pi^+$ events.

The fitted mean values of the Gaussian functions are $1866 \pm 3$ MeV/$c^2$ and $1863 \pm 2$ MeV/$c^2$ for the $\overline{\mathrm{D}}^0 \to \mathrm{K}^+\pi^-$ or $\mathrm{K}^+\pi^-\pi^-\pi^+$ decay modes, in good agreement with the nominal $\mathrm{D}^0$ mass [3], and the experimental resolutions are $26 \pm 3$ MeV/$c^2$ and $14 \pm 2$ MeV/$c^2$, respectively.

For $\mathrm{D}^{*-}\ell^+X$ events with $\mathrm{D}^{*-}$ decaying into $\overline{\mathrm{D}}^0\pi^-$ followed by $\overline{\mathrm{D}}^0 \to \mathrm{K}^+\pi^-$ or $\mathrm{K}^+\pi^-(\pi^0)$ , the mass difference distribution gives a better estimate of the number of $\mathrm{D}^{*-}\ell^+X$ candidates than the K$\pi$ mass distribution where the K$\pi(\pi^0)$ parameterization has to be taken into account. This is not the case for $\overline{\mathrm{D}}^0$ decays into $\mathrm{K}^+\pi^-\pi^-\pi^+$, because the kaon mass assignment can be permuted with a pion mass without greatly affecting the mass difference value. In the K3$\pi$ mode, the number of $\mathrm{D}^{*-}\ell^+X$ events is evaluated using the invariant mass distribution of figure 1d).

The mass difference distributions $M(\mathrm{K}^+\pi^-\pi^-) - M(\mathrm{K}^+\pi^-)$ are presented in figures 2a) and b) where the $\mathrm{K}^+\pi^-$ invariant mass is required to be within 50 MeV/$c^2$ of the nominal $\mathrm{D}^0$ mass in a), and between 1550 MeV/$c^2$ and 1700 MeV/$c^2$ in b). The data points and the hatched histograms represent the same charge and opposite charge K-lepton correlations in the same jet, respectively. The background is described by the function $\alpha(\Delta M - m_\pi)^\beta$ where $\alpha$ and $\beta$ are free parameters. In a) the $\mathrm{D}^{*-} \to (\mathrm{K}^+\pi^-)\pi^-$ signal is described by a Gaussian function with free normalization, mean value and width. The obtained mean value ($145.3 \pm 0.1$ MeV/$c^2$) is compatible with the expected ($\mathrm{D}^{*+} - \mathrm{D}^0$) mass difference value and the resolution is $0.9 \pm 0.1$ MeV/$c^2$. In b) the $\mathrm{D}^{*-} \to (\mathrm{K}^+\pi^-(\pi^0))\pi^-$ signal is fitted using two half-Gaussian functions with fixed parameters (according to the simulation), but free normalization. The two functions had a common central value but different widths on each side.

## 3.4 Final selection

In summary, the particle combination was considered as a $\overline{\mathrm{D}}^0\ell^+$ candidate if the mass difference $\Delta M$, for all possible $\overline{\mathrm{D}}^0\pi^-\ell^+$ combinations, differed by more than 2 MeV/$c^2$ from the nominal ($\mathrm{D}^{*+} - \mathrm{D}^0$) mass difference. For $\overline{\mathrm{D}}^0 \to \mathrm{K}^+\pi^-$ (or $\overline{\mathrm{D}}^0 \to \mathrm{K}^+\pi^-\pi^-\pi^+$) decay modes, the K$\pi$ (or K3$\pi$) invariant mass was required to be within $\pm 50$ MeV/$c^2$ (or $\pm 30$ MeV/$c^2$) of the nominal $\mathrm{D}^0$ mass.

The same criteria were used for $\mathrm{D}^{*-}\ell^+$ candidates, except that the mass difference had to lie within 2 MeV/$c^2$ of the nominal ($\mathrm{D}^{*+} - \mathrm{D}^0$) mass difference in case of a $\overline{\mathrm{D}}^0 \to \mathrm{K}^+\pi^-$ decay and within 1.5 MeV/$c^2$ in case of a $\overline{\mathrm{D}}^0 \to \mathrm{K}^+\pi^-\pi^-\pi^+$ decay. For $\overline{\mathrm{D}}^0 \to \mathrm{K}^+\pi^-(\pi^0)$ decay, the $\mathrm{K}^+\pi^-$ invariant mass was required to be between 1550 MeV/$c^2$ and 1700 MeV/$c^2$ and the mass difference to be less than 152 MeV/$c^2$.

Using these selections, the fitted numbers of $\overline{\mathrm{D}}^0\ell^+X$ and $\mathrm{D}^{*-}\ell^+X$ events are presented in tables 1 and 2, together with the observed signal fractions. An overall number of $377 \pm 28$ $\overline{\mathrm{D}}^0\ell^+$ and $309 \pm 22$ $\mathrm{D}^{*-}\ell^+$ candidates are available for the $\mathrm{B}^+$ and $\mathrm{B}^0$ lifetime measurements.

# 4 Average B lifetime using $\overline{\mathrm{D}}^0\ell^+$ and $\mathrm{D}^{*-}\ell^+$ samples

The $\overline{\mathrm{D}}^0\ell^+$ and $\mathrm{D}^{*-}\ell^+$ samples are dominated by $\mathrm{B}^+$ and $\mathrm{B}^0$ decays, respectively (see section 1). In this section the measurement of the B lifetime is described in these $\overline{\mathrm{D}}\ell^+$ samples separately and an average lifetime is obtained for $\mathrm{B}^+$ and $\mathrm{B}^0$ mesons. In the next section the $\mathrm{B}^+$ and $\mathrm{B}^0$ lifetimes will be evaluated individually.

The B meson mean lifetime was determined from maximum likelihood fits to the B proper time distributions of the $\overline{\mathrm{D}}^0\ell^+$ and $\mathrm{D}^{*-}\ell^+$ samples. For each event the B proper time was computed as :

$$t(\mathrm{B}) = m_{\mathrm{B}} \cdot L(\mathrm{B})/p(\mathrm{B}) \tag{2}$$

where $L(\mathrm{B})$ is the signed decay length in space and $p(\mathrm{B})$ is the momentum of the B meson.

The B momentum was evaluated from the measured momentum $p_{\mathrm{D}\ell}$ and invariant mass $M_{\mathrm{D}\ell}$ of the $\overline{\mathrm{D}}\ell^+$ pair. A specific sample of $\mathrm{B} \to \overline{\mathrm{D}}^0\ell^+\nu X$ decays (which included $\overline{\mathrm{D}}^*$ and $\overline{\mathrm{D}}^{**}$ transitions) was simulated, corresponding to more than 10 times the amount of data events. After applying the same selection criteria as for the real $\overline{\mathrm{D}}\ell^+$ data, the simulated sample was divided into 7 intervals of $p_{\mathrm{D}\ell}$ between 10 GeV/$c$ and 45 GeV/$c$. In each interval the B momentum was estimated as :

$$p(\mathrm{B}) = m_{\mathrm{B}} \cdot \frac{p_{\mathrm{D}\ell}}{M_{\mathrm{D}\ell}} \cdot f(p_{\mathrm{D}\ell}, M_{\mathrm{D}\ell}) \tag{3}$$

where, for each $p_{\mathrm{D}\ell}$ bin, $f(p_{\mathrm{D}\ell}, M_{\mathrm{D}\ell})$ is represented as a third order polynomial in $M_{\mathrm{D}\ell}$. The function was between 0.6 and 1.2 for all values of $p_{\mathrm{D}\ell}$ and $M_{\mathrm{D}\ell}$ used in the analysis. As explained in section 3.2, the invariant mass $\overline{\mathrm{D}}\ell^+$ was required to be between 2.80 GeV/$c^2$ and the B mass value. For $\mathrm{D}^{*-} \to (\mathrm{K}^+\pi^-(\pi^0))\pi^-$ candidates, the parameters of the function $f(p_{\mathrm{D}\ell}, M_{\mathrm{D}\ell})$ were appropriately tuned and the upper limit on $M_{\mathrm{D}\ell}$ was reduced to 5.14 GeV/$c^2$.

According to the simulation, the overall resolution on $p(\mathrm{B})$ was $\pm 12\%$, but its value varied from $\pm 20\%$ at low $\overline{\mathrm{D}}\ell^+$ momentum to $\pm 5\%$ in the high momentum region. Figure 3 presents, both for the data (dots) and the simulation (histogram), the estimated B momentum after background subtraction, but without acceptance and selection efficiency correction. These distributions are consistent with each other.

As the information from the microvertex detector was only available in the plane transverse to the beam axis, the coordinates of the primary and secondary vertices were taken in this transverse plane. The signed decay length of the B meson, $L_T(\mathrm{B})$, was measured in this plane as the distance from the primary vertex to the $\overline{\mathrm{D}}^0\ell^+$ vertex. This distance was given the same sign as the scalar product of the $\overline{\mathrm{D}}\ell^+$ momentum with the vector joining the primary to the secondary vertices in the transverse plane. Considering the polar angle, $\theta_{\mathrm{D}\ell}$, of the measured $\overline{\mathrm{D}}\ell^+$ momentum as a reliable estimate of the B direction, the B decay length was finally computed in space :

$$L(\mathrm{B}) = L_T(\mathrm{B})/\sin\theta_{\mathrm{D}\ell}\ . \tag{4}$$

Similarly the $\overline{\mathrm{D}}^0$ decay length was computed from the measured $\overline{\mathrm{D}}^0\ell^+$ and $\overline{\mathrm{D}}^0$ vertices. The overall resolutions were found to be $\pm 14\%$ of the average B decay length in space and $\pm 54\%$ of the average $\overline{\mathrm{D}}^0$ decay length.

Figure 4 shows the reconstructed B proper time as a function of its generated value in the simulation. No significant bias was observed.

The proper time distribution of the combinatorial background below the D meson signals was evaluated by selecting some event samples in the neighbourhood of the D mass, as displayed in table 3. These background samples were chosen in order to have kinematical conditions close to those of the selected $\overline{\mathrm{D}}\ell^+$ samples. According to the simulation their flavour composition was a good approximation to the real background below the signal of $\mathrm{B} \to \overline{\mathrm{D}}\ell^+\nu$ decays.

| | Background | | | |
|---|---|---|---|---|
| $\overline{\mathrm{D}}$ channel | sample | $M(\mathrm{K}(n)\pi))$ range (MeV/$c^2$) | $\Delta M$ range (MeV/$c^2$) | nb. of events |
| $\overline{\mathrm{D}}^0 \to \mathrm{K}\pi$ | $(\mathrm{K}^+\pi^-)\ell^-$ | $m_{\mathrm{D}^0} \pm 50$ | $\lvert\Delta m\rvert > 2$ | 167 |
| $\overline{\mathrm{D}}^0 \to \mathrm{K}3\pi$ | $(\mathrm{K}^+\pi^-\pi^-\pi^+)\ell^-$ | $m_{\mathrm{D}^0} \pm 30$ | $\lvert\Delta m\rvert > 2$ | |
| | $(\mathrm{K}^+\pi^-\pi^-\pi^+)\ell^+$ | $1760-1810, 1910-1950$ | $\lvert\Delta m\rvert > 2$ | 270 |
| $\mathrm{D}^{*-} \to (\mathrm{K}\pi)\pi$ | $(\mathrm{K}^+\pi^-)\pi^-\ell^-$ | $m_{\mathrm{D}^0} \pm 135$ | $< 160$ | 54 |
| $\mathrm{D}^{*-} \to (\mathrm{K}\pi(\pi^0))\pi$ | $(\mathrm{K}^+\pi^-)\pi^-\ell^-$ | $1550-1700$ | $160-200$ | 151 |
| $\mathrm{D}^{*-} \to (\mathrm{K}3\pi)\pi$ | $(\mathrm{K}^+\pi^-\pi^-\pi^+)\pi^-\ell^-$ | $m_{\mathrm{D}^0} \pm 30$ | $\lvert\Delta m\rvert < 3$ | |
| | $(\mathrm{K}^+\pi^-\pi^-\pi^+)\pi^-\ell^+$ | $1760-1810, 1910-1950$ | $\lvert\Delta m\rvert < 1.5$ | 107 |

Table 3: Selected right sign or wrong sign background samples for the B lifetime determination ($\Delta m$ is defined in table 1 caption).

An event-by-event maximum likelihood fit was performed on the proper time distribution of each $\overline{\mathrm{D}}\ell^+$ sample. The fitting function used two contributions :

- an exponential function convoluted with the experimental resolution, $\sigma_{t(\mathrm{B})}$, on the B decay length and, in case of the $\overline{\mathrm{D}}^0\ell^+$ sample where a $\Delta L/\sigma$ selection was applied, an acceptance correction estimated from the simulation;
- a function describing the proper time distribution of the background sample. The parameters of this function were fixed according to the fitted proper time distribution of the background sample.

The normalization factors of these two functions were fixed according to the observed signal fraction (see tables 1 and 2).

In a previous publication [5], the proper time distribution of the background sample was directly used in the likelihood fit. This method gives the same results as those presented in the following.

The fit was performed on all events with a proper time between $-2$ and $+10$ ps. The results are presented in figure 5a-e) and summarized in table 4 for each $\overline{\mathrm{D}}\ell^+$ channel.

As a cross-check of the lifetime measurement method and of the analysis procedure, the decay length between the measured $\overline{\mathrm{D}}^0$-lepton vertex and the measured $\overline{\mathrm{D}}^0$ vertex was used to fit the $\mathrm{D}^0$ lifetime (figure 5f). Here the proper time interval was between $-2$ and $+4$ ps. The value found was :

$$\tau(\mathrm{D}^0) = 0.443^{+0.021}_{-0.020}\ (\mathrm{stat.})\ \mathrm{ps}$$

in agreement with the world average value $0.415 \pm 0.004$ ps [3].

The B lifetime has been fitted in $\overline{\mathrm{D}}^0\ell^+X$ and $\mathrm{D}^{*-}\ell^+X$ samples, giving :

$$\begin{aligned} \tau(\mathrm{B}) &= 1.61^{+0.11}_{-0.10}\ (\mathrm{stat.})\ \pm 0.09\ (\mathrm{syst.})\ \mathrm{ps} \quad \text{where } \mathrm{B} \to \overline{\mathrm{D}}^0\ell^+X \\ \tau(\mathrm{B}) &= 1.61^{+0.11}_{-0.10}\ (\mathrm{stat.})\ \pm 0.06\ (\mathrm{syst.})\ \mathrm{ps} \quad \text{where } \mathrm{B} \to \mathrm{D}^{*-}\ell^+X \end{aligned}$$

| Figure | B decay | $\overline{\mathrm{D}}$ decay | B lifetime (ps) |
|---|---|---|---|
| 5b) | $\overline{\mathrm{D}}^0\ell^+X$ | $\overline{\mathrm{D}}^0 \to \mathrm{K}\pi$ | $1.60^{+0.15}_{-0.14}$ (stat.) |
| 5d) | $\overline{\mathrm{D}}^0\ell^+X$ | $\overline{\mathrm{D}}^0 \to \mathrm{K}3\pi$ | $1.65^{+0.18}_{-0.15}$ (stat.) |
| 5a) | $\mathrm{D}^{*-}\ell^+X$ | $\mathrm{D}^{*-} \to (\mathrm{K}\pi)\pi$ | $1.66^{+0.21}_{-0.18}$ (stat.) |
| 5e) | $\mathrm{D}^{*-}\ell^+X$ | $\mathrm{D}^{*-} \to (\mathrm{K}\pi(\pi^0))\pi$ | $1.55^{+0.20}_{-0.17}$ (stat.) |
| 5c) | $\mathrm{D}^{*-}\ell^+X$ | $\mathrm{D}^{*-} \to (\mathrm{K}3\pi)\pi$ | $1.62^{+0.19}_{-0.16}$ (stat.) |
| | $\overline{\mathrm{D}}^0\ell^+X$ | all $\overline{\mathrm{D}}^0$ | $1.61^{+0.11}_{-0.10}$ (stat.) |
| | $\mathrm{D}^{*-}\ell^+X$ | all $\mathrm{D}^{*-}$ | $1.61^{+0.11}_{-0.10}$ (stat.) |
| 6) | $\overline{\mathrm{D}}\ell^+X$ | all $\overline{\mathrm{D}}^0$ and $\mathrm{D}^{*-}$ | $1.61^{+0.08}_{-0.07}$ (stat.) |

Table 4: B lifetime measurements for the selected $\mathrm{B} \to \overline{\mathrm{D}}\ell^+X$ decays.

Both K$\pi$ and K3$\pi$ modes of the $\overline{\mathrm{D}}^0\ell^+$ sample were used in a combined fit and similarly K$\pi$, K$\pi(\pi^0)$ and K3$\pi$ modes for the $\mathrm{D}^{*-}\ell^+$ sample.

The full sample can also be used to determine an average lifetime of $\mathrm{B}^+$ and $\mathrm{B}^0$ mesons (figure 6) :

$$\tau(\mathrm{B}) = 1.61^{+0.08}_{-0.07}\ (\mathrm{stat.}) \pm 0.05\ (\mathrm{syst.})\ \mathrm{ps}.$$

The different contributions to the systematic uncertainty are summarized in table 5.

| Source of error | $\tau$(B) with $\overline{\mathrm{D}}^0\ell^+X$ | $\tau$(B) with $\mathrm{D}^{*-}\ell^+X$ | average $\tau$(B) | $\tau(\mathrm{B}^+)$ | $\tau(\mathrm{B}^0)$ | $\frac{\tau(\mathrm{B}^+)}{\tau(\mathrm{B}^0)}$ |
|---|---|---|---|---|---|---|
| Background estimate | $\pm$5.1 | $\pm$3.3 | $\pm$2.8 | $\pm$7.1 | $\pm$4.3 | $\pm$9.7 |
| $p$(B) estimate | $\pm$1.0 | $\pm$1.0 | $\pm$1.0 | $\pm$1.0 | $\pm$1.0 | — |
| Fit procedure | $\pm$1.2 | $\pm$1.8 | $\pm$1.0 | $\pm$1.8 | $\pm$2.3 | $\pm$3.5 |
| $\Delta L/\sigma$ selection of $\mathrm{D}^0$ | $\pm$1.0 | — | $\pm$0.7 | $\pm$1.4 | $\pm$0.2 | $\pm$1.6 |
| Error estimate on $\sigma_{t(\mathrm{B})}$ | $\pm$0.9 | $\pm$0.7 | $\pm$0.8 | $\pm$0.9 | $\pm$0.7 | — |
| Total | $\pm$5.5 | $\pm$4.0 | $\pm$3.3 | $\pm$7.6 | $\pm$5.0 | $\pm$10.4 |

Table 5: Contributions (%) to the systematic uncertainty of the measured B lifetimes and lifetime ratio.

The B lifetime was measured on a simulated sample of hadronic $\mathrm{Z}^0$ decays, repeating the same selections for the signal and for the background as in the data and following the same fitting procedure. The fitted B lifetimes of both $\overline{\mathrm{D}}^0\ell^+$ and $\mathrm{D}^{*-}\ell^+$ samples, $1.56 \pm 0.05$ ps and $1.67 \pm 0.06$ ps respectively, were found compatible with the mean generated value of 1.6 ps. The statistical error due to the background in these generated samples was $\pm 3\%$ which was used to estimate the error due to the choice of the background samples. A further uncertainty of $\pm 4\%$ was added in quadrature for the $\overline{\mathrm{D}}^0\ell^+$ sample in order to describe the background parameterization of the real data. This was evaluated by fitting for each $\overline{\mathrm{D}}\ell^+$ sample separately both the overall proper time distribution and those from the estimated background sample, letting free the parameters of the function for the background. This additional uncertainty was $\pm 1\%$ for the $\mathrm{D}^{*-}\ell^+$ sample where the background fraction is lower. Varying the estimated signal fraction within its statistical

error changed the fitted $B^+$ and $B^0$ lifetimes by $\pm 1\%$. The quadratic sum of these systematic uncertainties is indicated in the first line of table 5.

An uncertainty of $\pm 1.0\%$ on the B momentum due to the formula used in equation (3) was evaluated by comparing the estimated B average momentum in the data and in the simulation after background subtraction for the $\overline{D}^0\ell^+$ and $D^{*-}\ell^+$ samples separately. The uncertainty on the B momentum due to the $\overline{D}^{**}$ contribution in B semileptonic decays was estimated by varying this contribution by $\pm 40\%$ in the simulation. The resulting change on the B momentum was only $\pm 0.2\%$.

To investigate further systematic errors arising from the fit procedure and acceptance corrections, a specific sample of $B \to \overline{D}^0\ell^+\nu X$ simulated events was used with the same selections as the real data. The B lifetime value obtained was compatible with the generated mean lifetime. An uncertainty of $\pm 1\%$ to $\pm 2\%$ was estimated to describe the fit procedure, reflecting the statistical precision of this generated sample. This error describes the confidence in the calculation of the distance between the primary and $\overline{D}\ell^+$ vertices and the choice of the proper time interval (between -2 and +10 ps). No significant difference was observed in the data when varying the upper limit of the proper time interval between +8 and +12 ps.

The uncertainty due to the acceptance correction was evaluated by varying by $\pm 10\%$ the value of the $\Delta L/\sigma$ selection in the $\overline{D}^0\ell^+$ samples. This variation reflected some residual differences observed between data and simulation for the $\Delta L/\sigma$ and $\sigma$ distributions.

The error on the B proper time measurement, $\sigma_{t(\mathrm{B})}$, used in the likelihood function depends only on the B decay length precision. As above, an uncertainty due to the evaluation of this error was introduced by varying $\sigma_{t(\mathrm{B})}$ by $\pm 10\%$. This changed the measured B lifetime by less than $\pm 1\%$.

Part of the $\overline{D}\ell^+$ sample is produced by the decay $B \to \overline{D}^0 D X$, followed by a semileptonic decay of the D daughter, or by $\overline{D}$ mesons associated with a fake lepton in $c\overline{c}$ events. As a $p_T$ cut was applied, this contamination amounts to 1% of the events and the change in the measured B lifetime was found negligible in the simulation. Similarly the decay $B \to \overline{D}^0\tau^+\nu_\tau X$, where the electron or muon is issued from the $\tau$ decay, amounts for 1% of the events and does not significantly affect the B lifetime measurement.

# 5 $B^+$ and $B^0$ lifetimes

Inside the $\overline{D}\ell^+$ samples the relative proportions of $B^+$ and $B^0$ mesons have to be evaluated in order to determine the $B^+$ and $B^0$ lifetimes. A $B^+$ meson can decay into $\overline{D}^0\ell^+\nu$, $\overline{D}^{*0}\ell^+\nu$ or $\overline{D}^{**0}\ell^+\nu$. Similarly a $B^0$ meson can decay into $D^{(*)(*)-}\ell^+\nu$.

The $\overline{D}^{*0}$ decays into $\overline{D}^0$ final state, but the $D^{*-}$ may decay into $\overline{D}^0$ or $D^-$ according to the branching ratio $Br(D^{*-} \to \overline{D}^0\pi^-) = 0.681 \pm 0.016$ [11]. From the simulation, the probability to miss the pion from a $D^{*-} \to \overline{D}^0\pi^-$ decay is $0.18 \pm 0.02$ when the $\overline{D}^0$ is reconstructed in the $K\pi$ or $K3\pi$ channels.

The $\overline{D}^{**}$ states can decay into a $\overline{D}$ or $\overline{D}^*$ final state. The convolution of the $\overline{D}^{**}$ amounts and branching ratios with the $D^{*-}$ reconstruction efficiency induces different fractions of initial $B^+$ and $B^0$ decays in the $\overline{D}^0\ell^+X$ and $D^{*-}\ell^+X$ samples.

Only narrow P-wave states have been observed [3][12][13] and the overall $B \to \overline{D}^{**}\ell^+\nu$ branching ratio has only been quoted in a single experiment [14]. This branching ratio will thus be estimated assuming that B semileptonic decays are saturated with $\overline{D}$, $\overline{D}^*$ and $\overline{D}^{**}$ transitions.

From the $B^0$ branching ratios measured at the $\Upsilon(4S)$ energy [3] :

$$\begin{aligned} Br(B^0 \to X\ell^+\nu) &= (9.5 \pm 1.6)\% \\ Br(B^0 \to D^-\ell^+\nu) &= (1.9 \pm 0.5)\% \\ Br(B^0 \to D^{*-}\ell^+\nu) &= (4.4 \pm 0.4)\% \ , \end{aligned}$$

the branching ratio $Br(B^0 \to D^{**-}\ell^+\nu) = (3.2 \pm 1.7)\%$ is inferred. The fraction of $B^0$ semileptonic decays involving a $\overline{D}^{**}$ is thus estimated to be $0.34 \pm 013$. Assuming equal partial widths for $B^+$ and $B^0$ semileptonic decays, then the $B^+$ semileptonic branching ratios are simply obtained from the relation :

$$Br(B^+ \to \overline{D}^{(*)(*)0}\ell^+\nu) = \frac{\tau(B^+)}{\tau(B^0)} \cdot Br(B^0 \to D^{(*)(*)-}\ell^+\nu) \ . \qquad (5)$$

However due to the lepton transverse momentum and $\overline{D}\ell^+$ invariant mass selections, the probability to reconstruct a $\overline{D}\ell^+$ coming from a $B \to \overline{D}^{**}\ell^+\nu$ decay is lower than if the primary charm meson was a $\overline{D}$ or a $\overline{D}^*$. The reduction factor is $0.77 \pm 0.04$ according to the simulation.

The average $D^{**}$ branching ratio into $D^*\pi$ was taken to be $0.5 \pm 0.3$, in agreement with a recent measurement [12].

The relative amounts of $B^+$ and $B^0$ mesons inside the $\overline{D}^0\ell^+X$ and $D^{*-}\ell^+X$ samples can then be inferred from these previous results, using the same hypothesis as in the appendix of reference [5].

As in the previous section, an event-by-event maximum likelihood fit was performed on the proper time distribution of all $\overline{D}\ell^+$ samples where the $B^+$ and $B^0$ mean lifetimes were free parameters. The charged and neutral B meson lifetimes are found to be :

$$\begin{aligned} \tau(B^+) &= 1.61^{+0.16}_{-0.16}\ (\text{stat.}) \pm 0.12\ (\text{syst.})\ \text{ps} \\ \tau(B^0) &= 1.61^{+0.14}_{-0.13}\ (\text{stat.}) \pm 0.08\ (\text{syst.})\ \text{ps} \\ \tau(B^+)/\tau(B^0) &= 1.00^{+0.17}_{-0.15}\ (\text{stat.}) \pm 0.10\ (\text{syst.}) \end{aligned}$$

where the systematic uncertainties are detailed in table 5.

The proportion of $B^+$ semileptonic decays in the $\overline{D}^0\ell^+X$ sample is $0.76 \pm 0.07$ and that of $B^0$ in the $D^{*-}\ell^+X$ sample is $0.85 \pm 0.10$ where the error reflects the uncertainty on the previous B, $\overline{D}^{**}$ and $D^{*-}$ branching ratios and on the $\overline{D}^{**}$ and $D^{*-}$ selection efficiencies. The magnitude of these diluting factors induces a larger statistical error for the $B^+$ and $B^0$ lifetimes than for the lifetime of the individual $\overline{D}^0\ell^+$ and $D^{*-}\ell^+$ samples. The uncertainty on these factors induces an additional systematic error in the $B^+$ and $B^0$ lifetimes and lifetime ratio, which cancels when the lifetime ratio is close to unity.

# 6 Conclusion

A sample of $377 \pm 28$ $\overline{D}^0\ell^+$ and $309 \pm 22$ $D^{*-}\ell^+$ events was reconstructed using DELPHI data collected in 1991-1993. The lepton was selected with a high transverse momentum in the same jet and with the same charge as the kaon from D decay. These events mainly originate from $B^+$ and $B^0$ semileptonic decays.

The B decay length was measured using the microvertex detector information and the B momentum was estimated from the observed $\overline{D}\ell^+$ invariant mass and momentum. An average lifetime is obtained for $B^+$ and $B^0$ mesons :

$$\tau(B) = 1.61^{+0.08}_{-0.07}\ (\text{stat.}) \pm 0.05\ (\text{syst.})\ \text{ps}.$$

Estimating the $B^0 \to D^{**-}\ell^+\nu$ branching ratio and the fraction of $D^{**}$ decay into $D^*\pi$, the lifetimes of charged and neutral B mesons are determined :

$$\begin{aligned} \tau(B^+) &= 1.61^{+0.16}_{-0.16}\ (\text{stat.}) \pm 0.12\ (\text{syst.})\ \text{ps} \\ \tau(B^0) &= 1.61^{+0.14}_{-0.13}\ (\text{stat.}) \pm 0.08\ (\text{syst.})\ \text{ps} \\ \tau(B^+)/\tau(B^0) &= 1.00^{+0.17}_{-0.15}\ (\text{stat.}) \pm 0.10\ (\text{syst.}). \end{aligned}$$

The $B^+$ and $B^0$ lifetimes are found equal within errors. This result is in agreement with the naive spectator model and with a recent theoretical evaluation where corrections to the spectator model are taken into account [2]. It also agrees with indirect measurements at the $\Upsilon(4S)$ energy using the ratio of $B^0$ and $B^+$ semileptonic branching fractions [15] and with published B lifetimes [5] [16].

These results replace those obtained from a previous DELPHI publication [5] which was based on the 1991 data only.

## Acknowledgements

We are greatly indebted to our technical collaborators and to the funding agencies for their support in building and operating the DELPHI detector, and to the members of the CERN-SL Division for the excellent performance of the LEP collider.

# References


[1] H. Fritzsch and P. Minkowski: Phys. Rep. **73** (1981) 67.

[2] I. Bigi et al., "Non Leptonic Decays of Beauty Hadrons – From Phenomenology to Theory", CERN–TH.7132/94 (1994), published in "B decays" $2^{nd}$ed., S. Stone (ed.), Word Scientific.

[3] Particle Data Group, "Review of Particle Properties", Phys. Rev. **D50**, Part I (1994).

[4] P. Roudeau, Proc. XXVII International Conference on High Energy Physics, Glasgow, 20-27 July 1994, p. 325.

[5] P. Abreu et al. (DELPHI Collab.), Zeit. Phys. **C57** (1993) 181.

[6] P. Aarnio et al. (DELPHI Collab.), Nucl. Inst. & Meth. **A303** (1991) 233.

[7] N. Bingefors et al., Nucl. Instr. & Meth. **A328** (1993) 447.

[8] E. G. Anassontzis et al., Nucl. Instr. & Meth. **A323** (1992) 351.

[9] T. Sjöstrand: Comp. Phys. Comm. **39** (1986) 347;
T. Sjöstrand and M. Bengtsson: Comp. Phys. Comm. **43** (1987) 367;
T. Sjöstrand: JETSET 7.3 manual, CERN-TH 6488/92 (1992).

[10] DELSIM Reference Manual, DELPHI 87-98 PROG 100, Geneva, July 1989.

[11] F. Butler et al. (CLEO Collab.), Phys. Rev. Lett. **69** (1992) 2041.

[12] D. Buskulic et al. (ALEPH Collab.), Phys. Lett. **345B** (1995) 103.

[13] R. Akers et al. (OPAL Collab.), "A study of Charm Meson Production in Semileptonic B Decays", CERN–PPE/95–02, Zeit. Phys. **C** to be published.

[14] H. Albrecht et al. (ARGUS Collab.), Zeit. Phys. **C57** (1993) 533.

[15] R. Fulton et al. (CLEO Collab.), Phys. Rev. **D43** (1991) 651;
H. Albrecht et al. (ARGUS Collab.), "Exclusive Semileptonic Decays of B Mesons to D Mesons", preprint DESY 92-029 (1992).

[16] D. Buskulic et al. (ALEPH Collab.), Phys. Lett. **307B** (1993) 194;
P.D. Acton et al. (OPAL Collab.), Phys. Lett. **307B** (1993) 247;
P. Abreu et al. (DELPHI Collab.), Phys. Lett. **312B** (1993) 253;
F. Abe et al. (CDF Collab.), Phys. Rev. Lett. **72** (1994) 3456;
R. Akers et al. (OPAL Collab.), "Improved measurements of the $B^0$ and $B^+$ meson lifetimes", CERN-PPE/95-19 (1995).

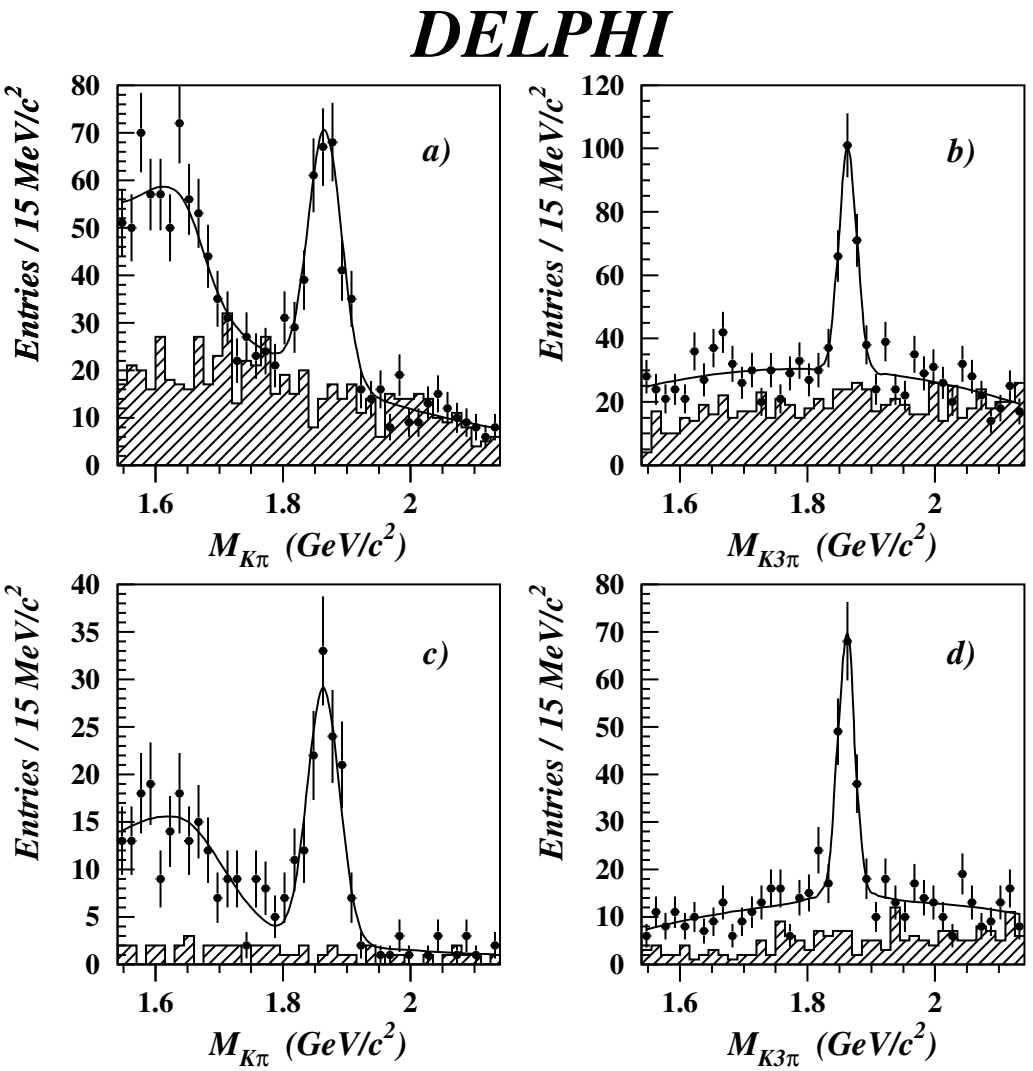


Figure 1: (a,c) $K^+\pi^-$ and (b,d) $K^+\pi^-\pi^-\pi^+$ invariant mass distributions from events containing a lepton in the same jet. Events from $D^{*-} \to \overline{D}^0\pi^-$ decays are rejected in (a,b) and selected in (c,d). The data points were obtained from events where the kaon candidate and the associated lepton have the same charge. The hatched histograms display the opposite charge kaon-lepton events where the same selections as for the same charge events are applied, except in a) where kaon identification is required. The curves are the results of fits described in the text.

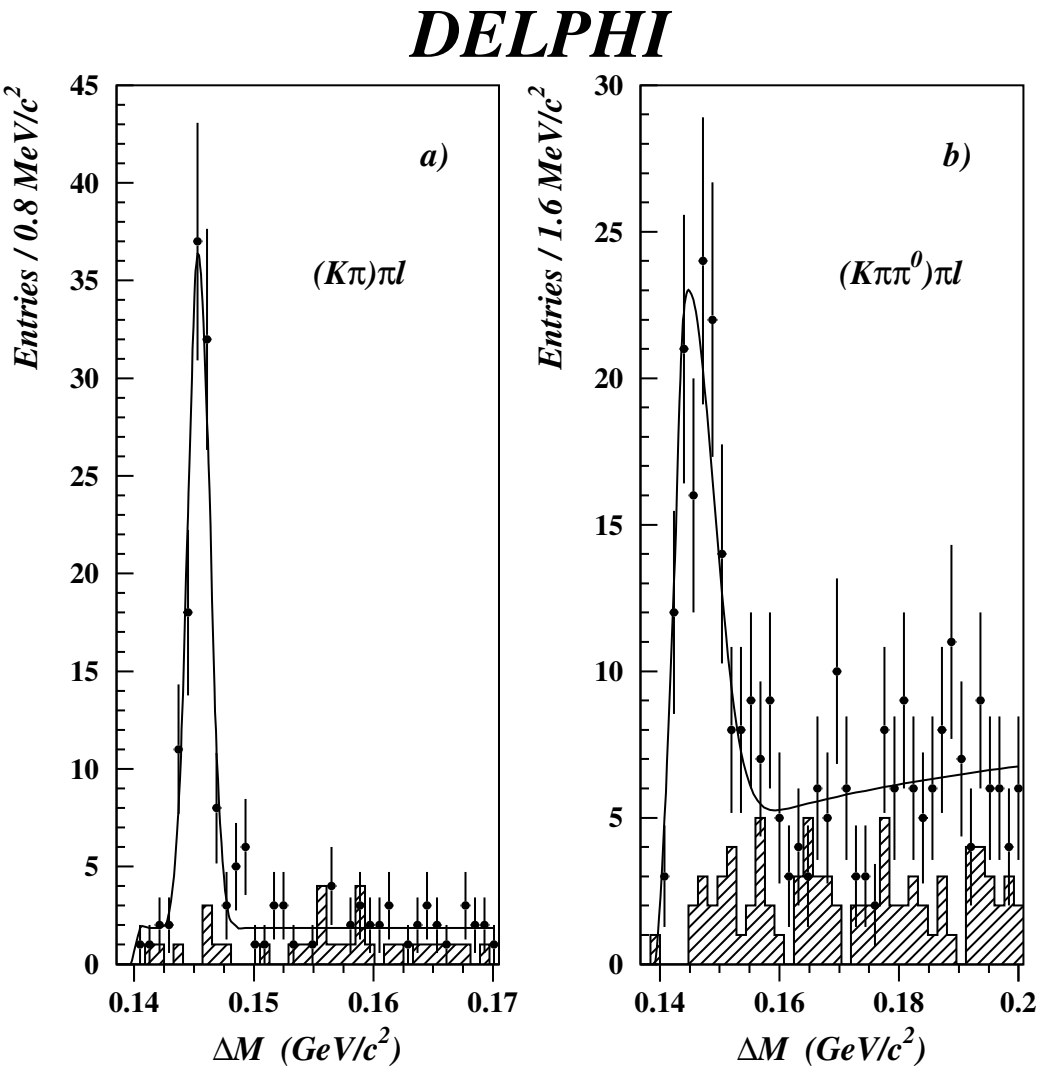


Figure 2: $\Delta M = M(\mathrm{K}^+\pi^-\pi^-) - M(\mathrm{K}^+\pi^-)$ distributions for events where the kaon candidate and the associated lepton in the same jet have the same charge (data points) or opposite charge (hatched histograms). A selection on $\mathrm{K}\pi$ mass within 50 MeV/$c^2$ of the nominal $\mathrm{D}^0$ mass is applied in a), and between 1550 MeV/$c^2$ and 1700 MeV/$c^2$ in b). The same selections are applied for the same and opposite charge events. The curves are the results of fits described in the text.

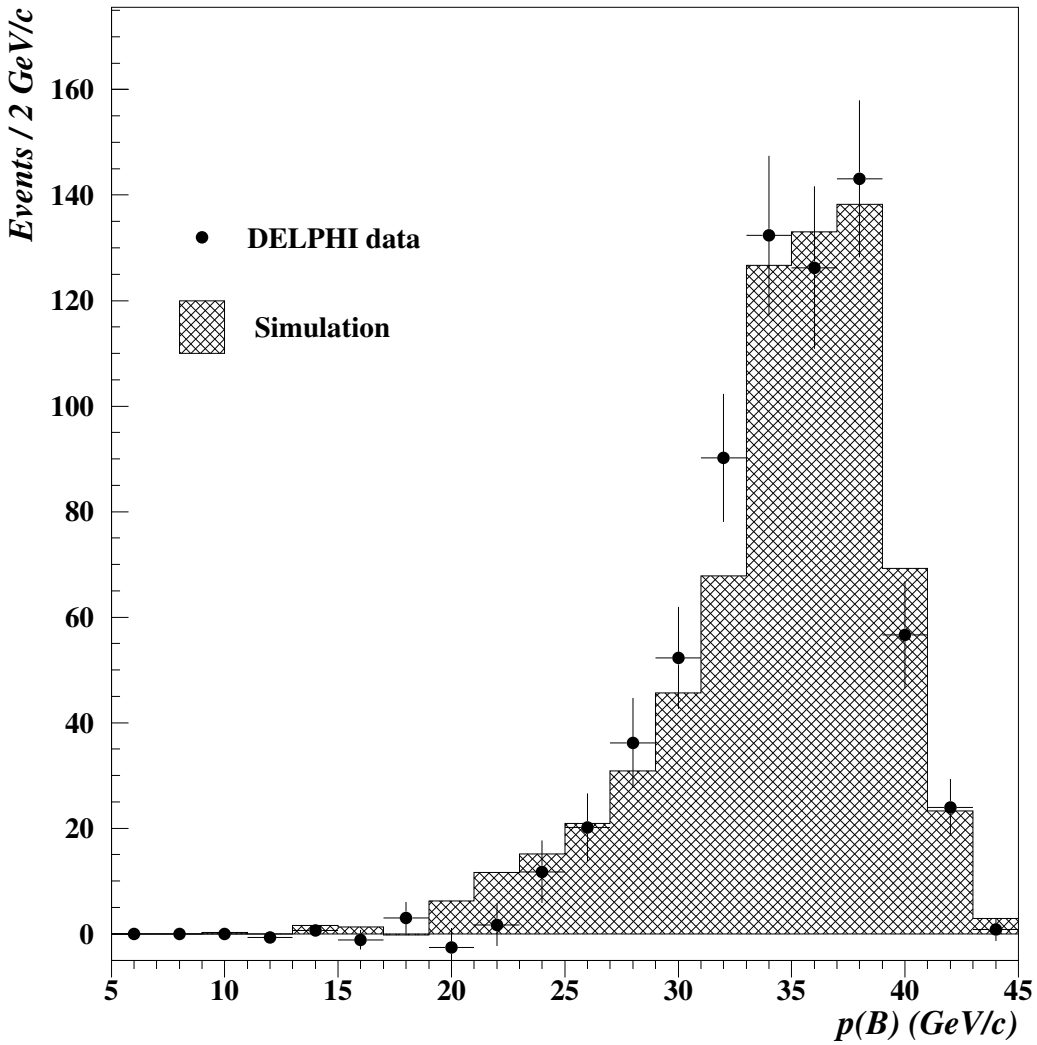


Figure 3: Raw distribution of the estimated B momentum after background subtraction in the data (dots) and in the simulation (histogram). All $\overline{\mathrm{D}}^0\ell^+$ and $\mathrm{D}^{*-}\ell^+$ samples using K$\pi$ and K3$\pi$ modes have been used. Only the statistical error in the data is presented. The simulation corresponds to three times more hadronic events than in the data.

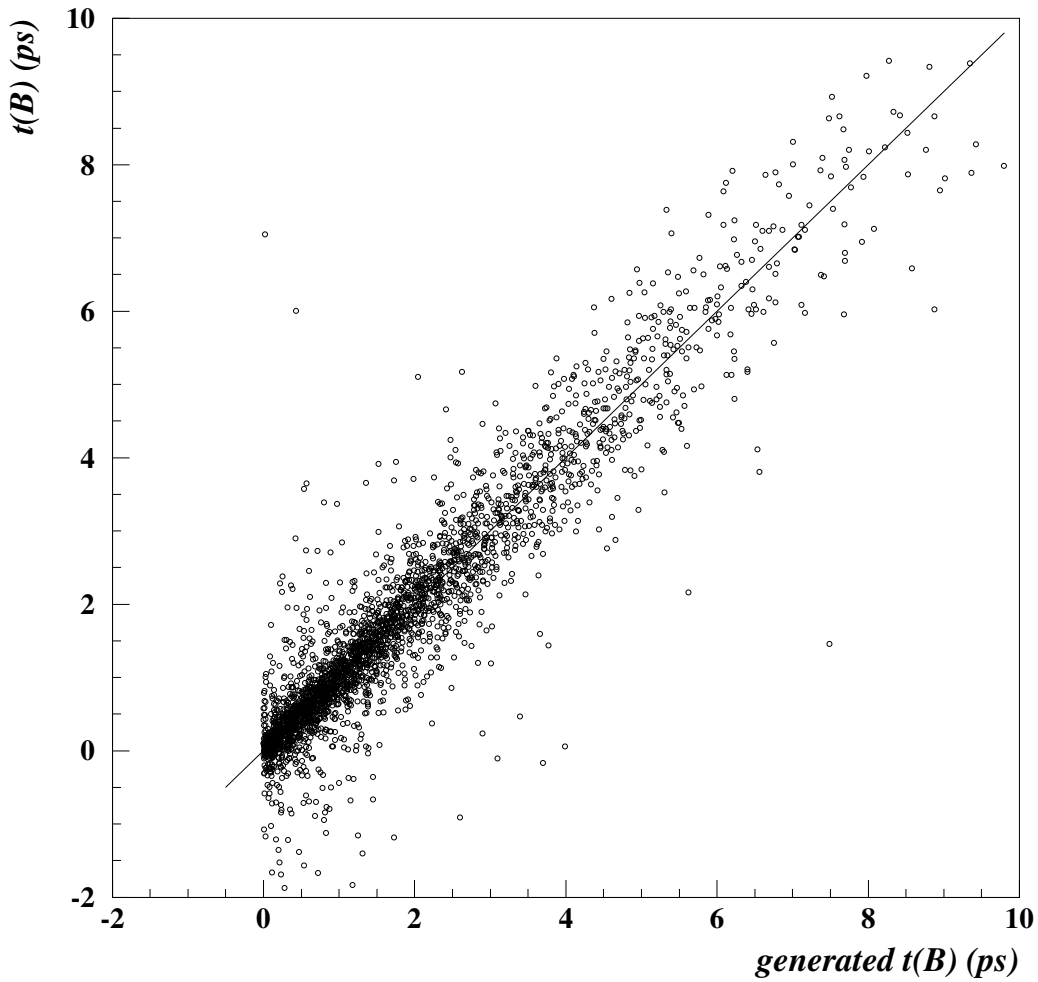


Figure 4: Reconstructed B proper time versus the generated B proper time in a simulated sample of $B \to \overline{D}^0 \ell^+ \nu X$ decays.

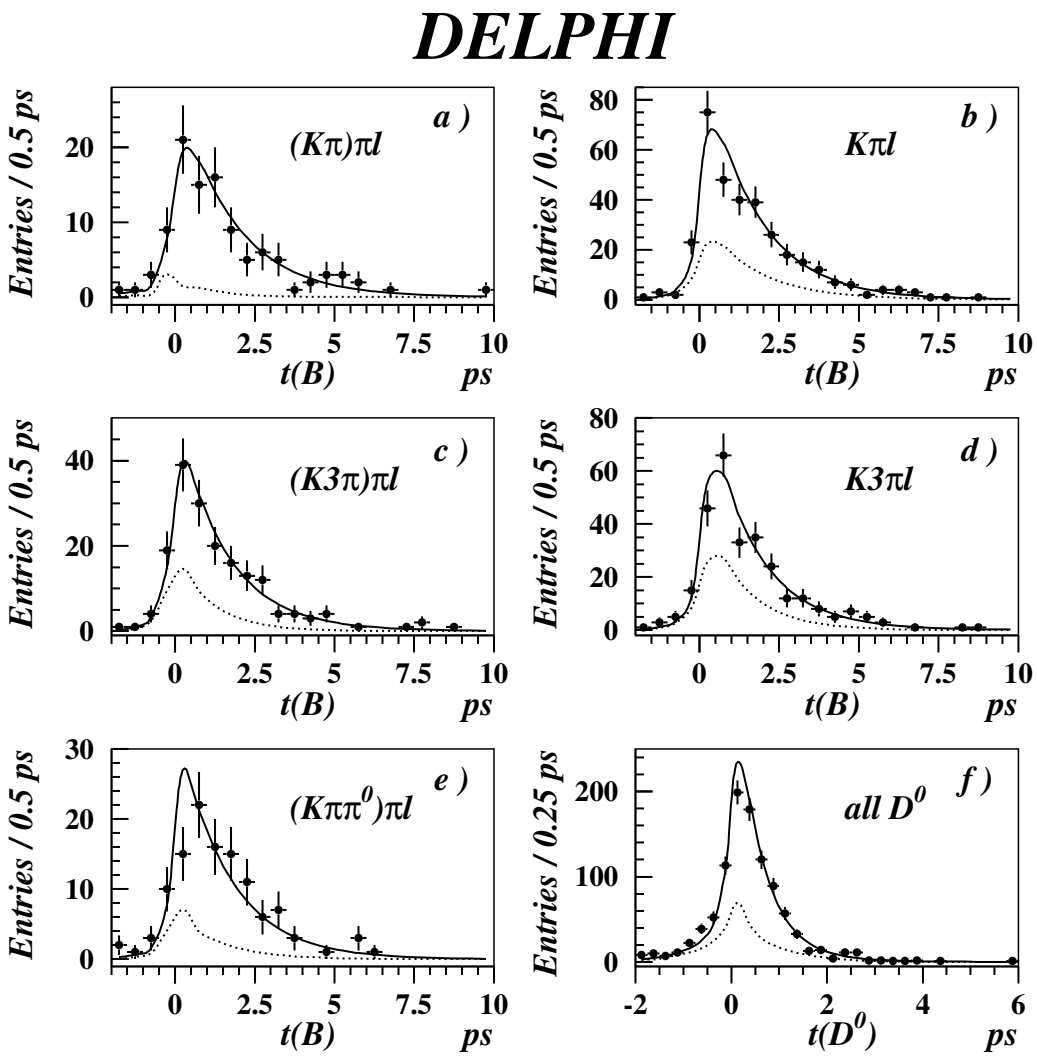


Figure 5: (a-e) B proper time distributions of each $\overline{\mathrm{D}}\ell^+$ sample and (f) $\mathrm{D}^0$ proper time distribution of all samples : signal plus background events (data points), estimated background contribution (dotted curve) and overall fitted function (solid curve).

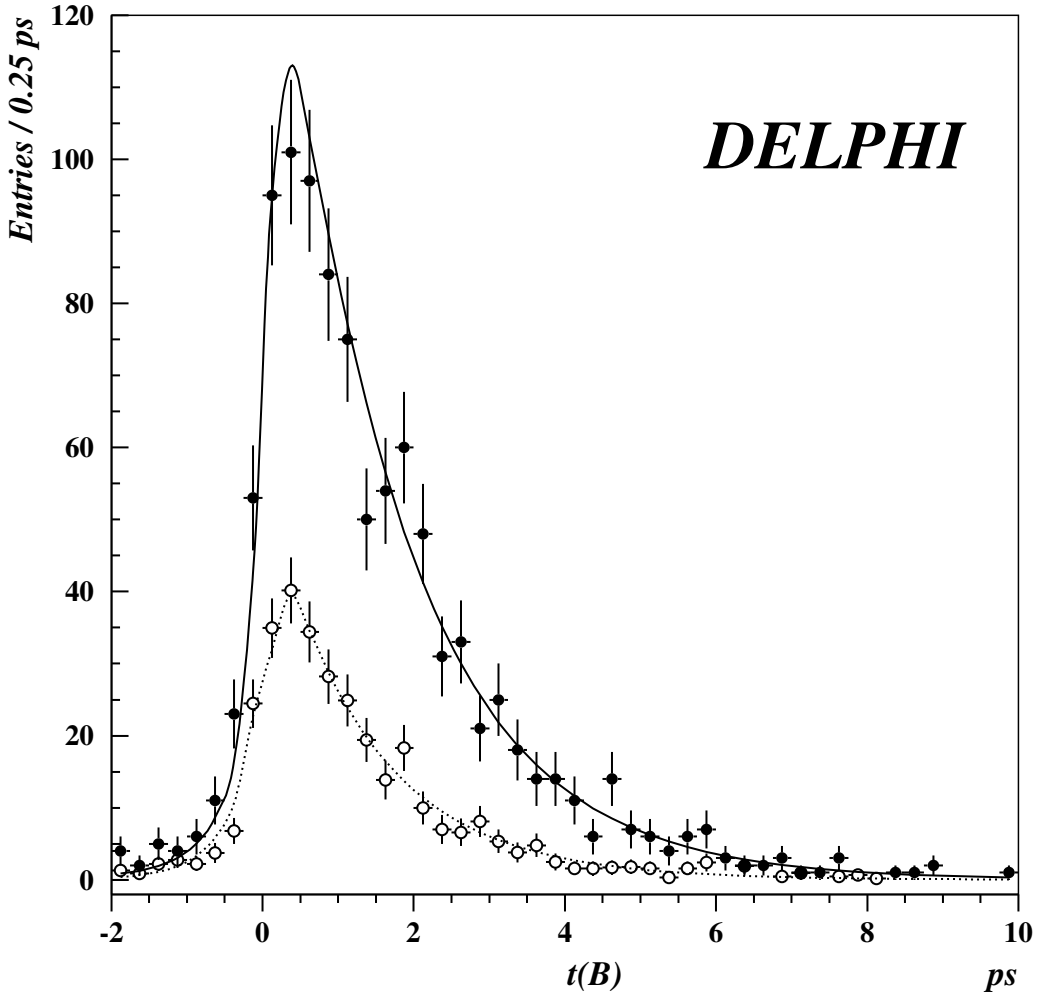


Figure 6: B proper time distribution of all $\overline{\mathrm{D}}\ell^+$ samples : signal plus background events (data points), normalized background sample (open circles), estimated background contribution (dotted curve) and overall fitted function (solid curve).